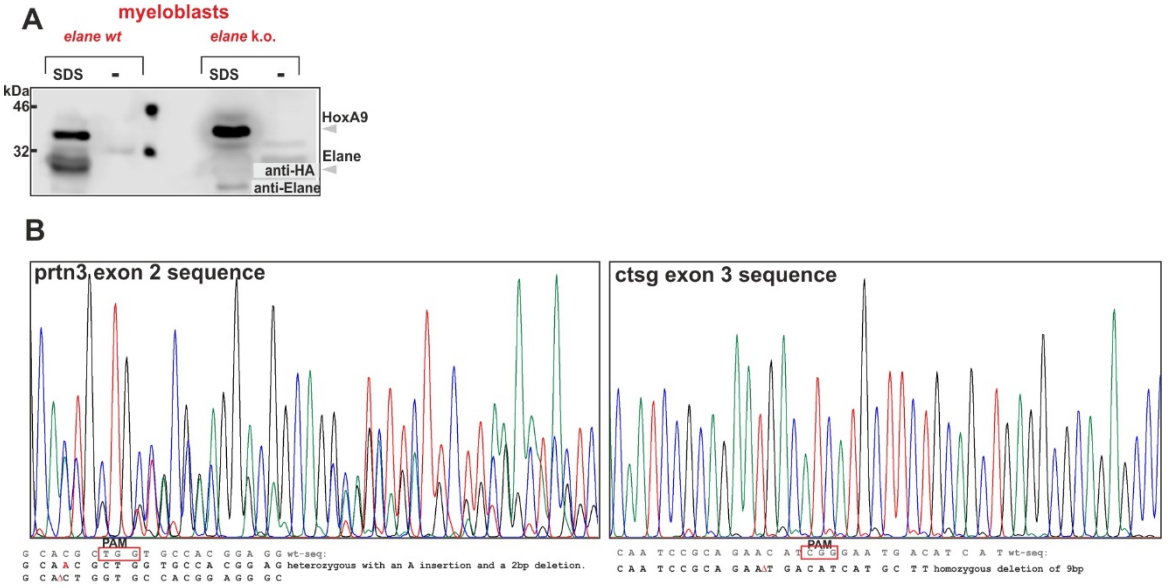

Zhong supplemental figure 1

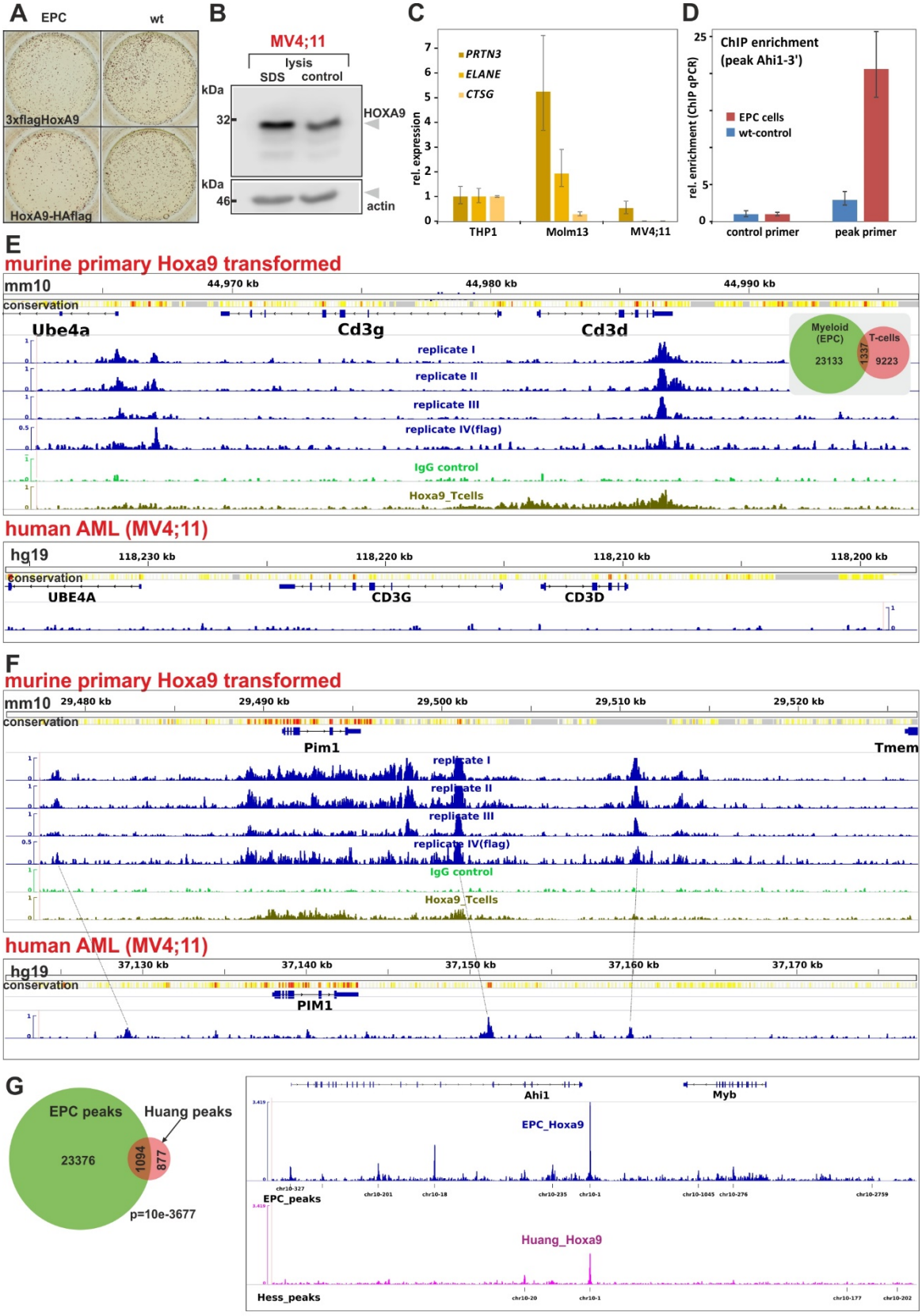

Zhong supplemental figure 2

A

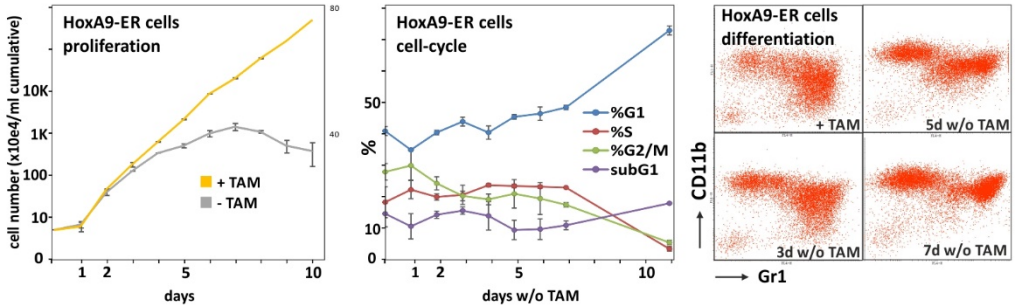

B

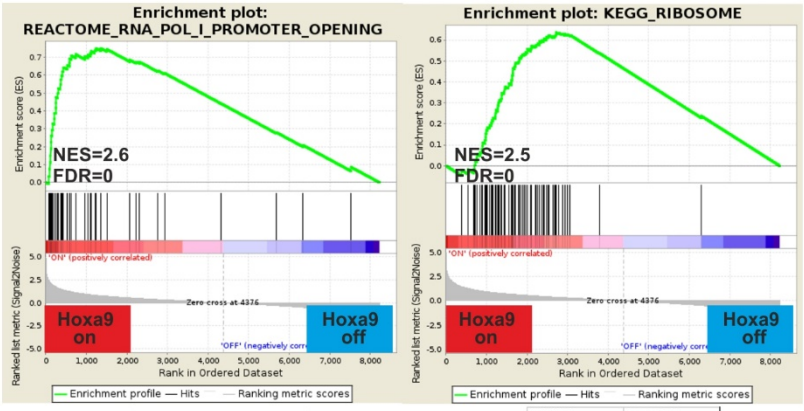

top 40 driver genes

NAME	PROBE
row_0	HIST4H4
row_1	HIST1H2BK
row_2	HIST1H3A
row_3	HIST1H3H
row_4	HIST1H3I
row_5	HIST1H4A
row_6	HIST1H2AD
row_7	HIST1H4B
row_8	HIST1H3D
row_9	HIST1H2BE
row_10	HIST1H2BC
row_11	HIST1H4J
row_12	HIST1H3E
row_13	HIST1H2BL
row_14	HIST1H2AE
row_15	HIST1H3G
row_16	HIST1H2BM
row_17	HIST1H2BH
row_18	HIST1H4H
row_19	HIST1H3F
row_20	HIST1H3C
row_21	HIST1H2AC
row_22	HIST1H4C
row_23	HIST1H2AB
row_24	HIST1H4K
row_25	HIST1H2BB
row_26	HIST2H2AC
row_27	HIST1H4I
row_28	HIST1H2BJ
row_29	HIST1H4D
row_30	HIST1H2BF
row_31	HIST1H4F
row_32	HIST1H2BG
row_33	HIST1H2BN
row_34	HIST1H3B
row_35	H2AFX
row_36	H3F3A
row_37	H2AFZ
row_38	UBTF
row_39	H3F3B
row_40	MBD2
row_41	HIST2H2BE
row_42	MAPK3

NAME	PROBE
row_0	RPS20
row_1	RPS28
row_2	RPL34
row_3	RPL10A
row_4	RPL3
row_5	RPL36
row_6	RPLP2
row_7	UBA52
row_8	RPL30
row_9	RPL23A
row_10	RPL22L1
row_11	RPL19
row_12	RPL7
row_13	RPS11
row_14	RPLP0
row_15	RPL27A
row_16	RPS29
row_17	RPS9
row_18	RPL29
row_19	RPL28
row_20	RPS2
row_21	RPL21
row_22	RPS26
row_23	RPS5
row_24	RPL17
row_25	RPL12
row_26	RPS16
row_27	RPS24
row_28	RPS21
row_29	RPL15
row_30	RPS13
row_31	RPS10
row_32	RPLP1
row_33	RPL13
row_34	RPS25
row_35	RPS15A
row_36	RPL8
row_37	RPS7
row_38	RPL35A
row_39	RPL11

Zhong supplemental figure 3

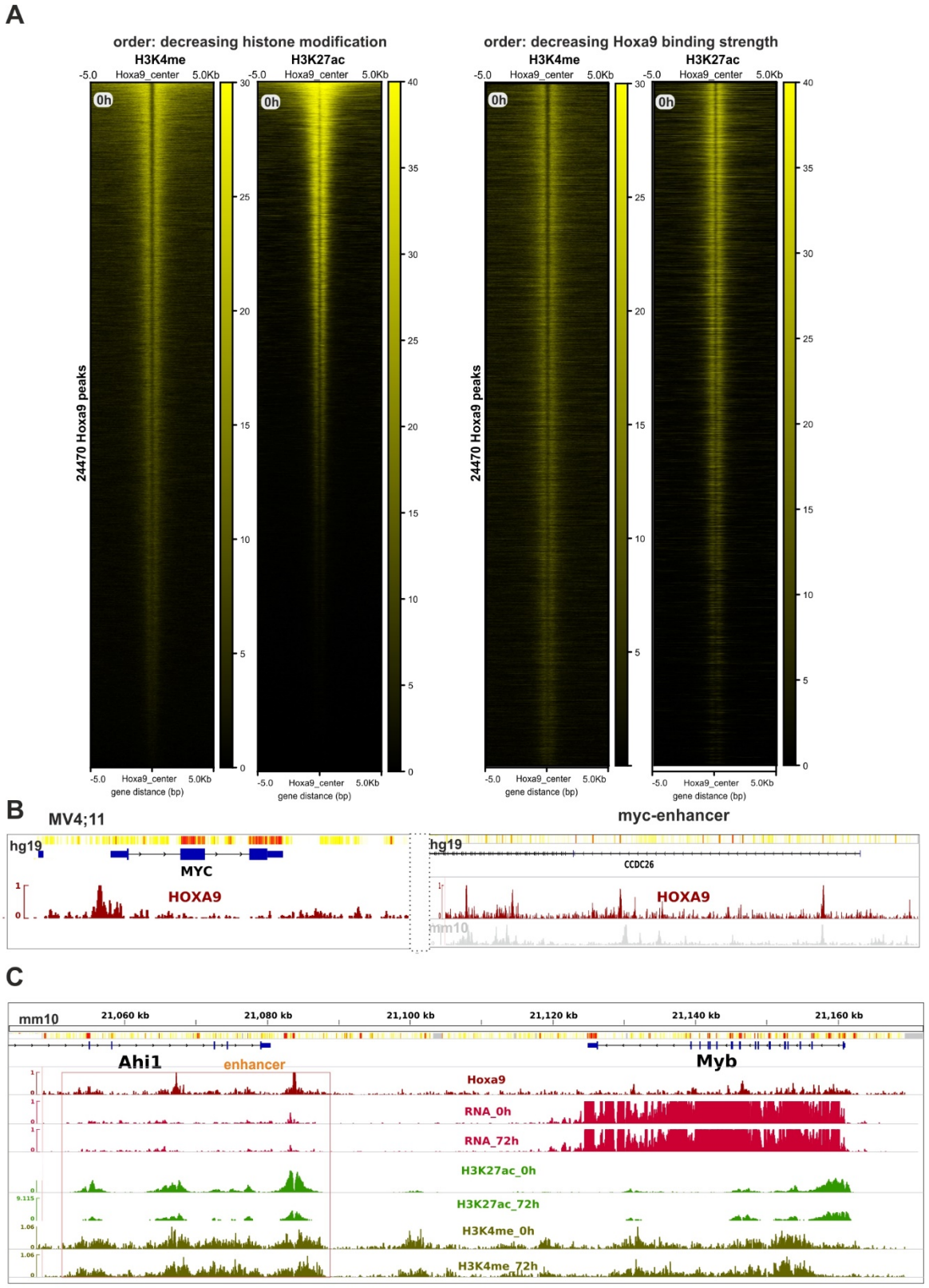

Zhong supplemental figure 4

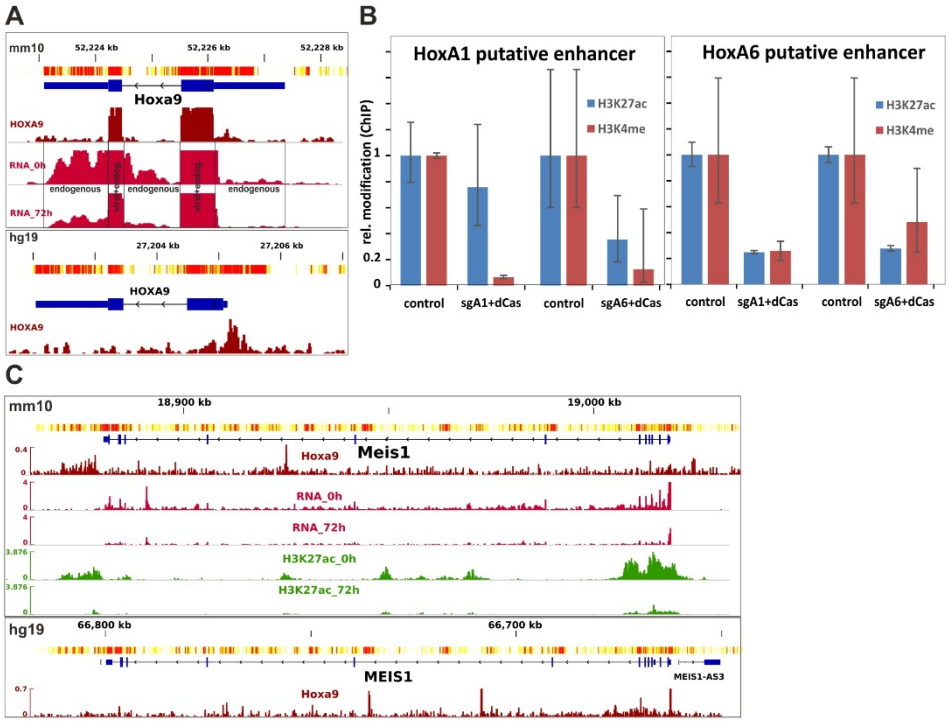

Zhong supplemental figure 5

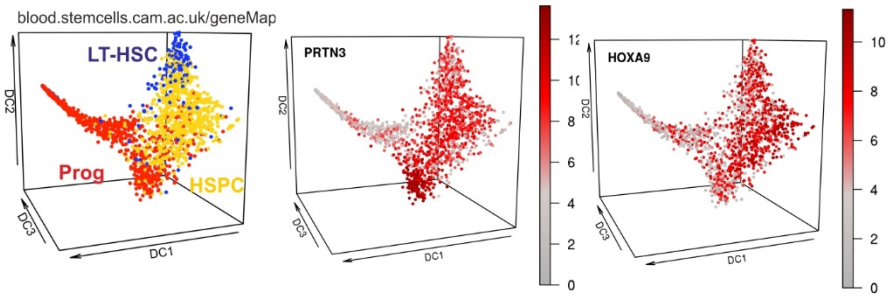

Zhong supplemental figure 6

Legends to supplemental figures

Supplemental figure 1: Degradation of HoxA9 by granule proteases

A: *Elane*$^{-/-}$ cells still degrade HoxA9. Western blot of extracts from myeloblasts derived from *Elane*$^{-/-}$ animals by HoxA9 transformation and analyzed for presence of HoxA9 and Elane. Wt cells are included as controls.

B: Sequences detecting deletions in single-cell cloned Crispr lines targeting *Prtn3* and *Ctsg*.

Supplemental figure 2: *Elane/Prtn3/Ctsg* triple knock-out myeloblasts (EPC) enable efficient ChIP of HoxA9

A: Representative example for a CFC replating assay done with EPC and wt primary HSPCs transformed by HoxA9. Stained colonies after two rounds of replating are shown for two differently tagged HoxA9 constructs as indicated.

B: HOXA9 is stable in extracts of human MV4;11 AML cells. Western blot detecting HOXA9 in triton lysates of MV4;11 cells incubated on ice for 10 min or boiled directly in SDS.

C: Granule protease RNA expression in human AML cell lines. *ELANE*, *PRTN3*, and *CTSG* RNA was quantified in THP1, Molm13, and MV4;11 cells by qPCR. Values are plotted relative to THP1.

D: Granule proteases degrade HoxA9 during ChIP procedure. An anti-flag ChIP was performed in parallel under identical conditions in EPC and wt cells transformed by 3xflagHoxA9. Efficiency of precipitation was determined by qPCR with primers for a control region not bound by HoxA9 and primers specific for the strong HoxA9 peak immediately downstream of *Ahi1*. Data are normalized to input.

E: HoxA9 binds cell-type specific to the CD3 TCR locus. IGV plot showing HoxA9 binding in 4 replicates of murine myeloblasts and in MV4;11 cells in comparison to the HoxA9 binding pattern in T-cells [31] . The inset depicts a Venn diagram counting overlapping and unique peaks for each cell-type.

F: Species and cell type conserved binding of HoxA9 to the *Pim1* locus. For clarity correlation between the tripartite enhancer structure in mouse and human samples is connected by lines.

G: Comparison of EPC ChIP results with previous data from Huang et al. [18] Left panel: Venn diagramm. Raw data of Huang et al. were analyzed with the same parameters as for the current ChIP experiments and resulting overlapping and unique peaks are plotted. Right panel: Peak calling around the confirmed HoxA9 target *Myb* demonstrates increased detection sensitivity for ChIP done in EPC cells.

Supplemental figure 3: GSEA of the HoxA9 regulatory pattern.

A: Characterization of HoxA9-ER cells after cessation of HoxA9 activity. Triplicate samples of HoxA9-ER cells were sampled in the presence of tamoxifen and during a time course (as indicated) after the inductor was removed. Proliferation was determined by cell counting, cell cycle analysis was done by standard propidium-iodide staining. For FACS analysis only one representative example is shown.

B: Two examples of gene expression patterns with significant similarity to the HoxA9 induced signatures. Both are driven through the strong regulation of histone and ribosomal protein genes by HoxA9.

Supplemental figure 4: HoxA9 binds to enhancers and promoters

A: Global correlation of HoxA9 binding and H3K4me/H3K27ac modification. The occupation plots show H3K4 mono-methylation and H3K27 acetylation in a region +/- 5kb around all identified murine HoxA9 peaks. The sort order is either according to modification intensity (left panels) or determined by decreasing HoxA9 peak-strenth (right panels).

B: Species conserved HoxA9 binding pattern to the promoter/gene region and the known downstream enhancer in MV4;11 cells.

C: A HoxA9 regulated putative enhancer for *Myb* within the *Ahi1* locus. The IGV tracks depict HoxA9 occupancy as well as nascent RNA reads, H3K27ac, H3K4me at 0h and 72h after cessation of HoxA9 activity. A potential enhancer structure is boxed. Note that the scale of the RNA tracks was adjusted so that enhancer RNAs become visible.

Supplemental figure 5: HoxA9 regulates itself and *Meis1*.

A: Detail of HoxA9 binding and RNA production in murine and MV4;11 cells around the HoxA9 coding region. Viral (exon) sequences and regions exclusively transcribed from the endogenous locus are boxed and labeled.

B: Epigenetic editing changes H3K4me and H3K27ac modification at the putative HoxA1 and HoxA6 enhancers. HoxA9 transformed cells expressing a catalytically inactive ("dead") Cas9 protein fused to the KRAB repressor domain and a sgRNA targeting this chimeric repressor to the putative HoxA1 and HoxA6 enhancers were used for H3K27ac and H3K4me specific ChIP experiments. Modification levels at the center of the respective enhancer region were measured by qPCR and are given as relative values compared to control cells without sgRNA.

C: HoxA9 regulatory situation at the *Meis1* locus in murine and human cells.

Supplemental figure 6: Expression of *HoxA9* and *Prtn3* during murine hematopoietic differentiation